A new indicator designed from the spectral coherence, proposition and application to bearing diagnosis

Souhayb KASS[1,2], Amani RAAD[2], Jérôme Antoni[1]

[1] Laboratoire Vibrations Acoustique, Univ Lyon, INSA-Lyon, LVA EA677, F-69621 Villeurbanne, France, e-mail : ***jerome.antoni@insa-lyon.fr***

[2] Engineering faculty, Lebanese University, Tripoli, Lebanon

1 Abstract

In vibration-based diagnosis of rolling element bearings, the complexity of the signals requires an expert to use advanced signal processing tools and to interpret the results based on his/her experience. Recently, a few autonomous methods have been proposed to alleviate the demand on the user's expertise, yet they have been mainly focused on fault detection. They ideally track certain properties in the signal, whose occurrence is correlated with the symptom of a fault. This paper follows a similar direction but with wider objectives: it aims to develop an indicator that is sensitive to both non-stationarity, non-Gaussianity and to the modification of the acoustic signature of the vibratory signal. The indicator is based on the recently developed Fast Spectral Coherence, a key tool of the theory of second-order cyclostationary processes. It condenses the whole information initially displayed in three dimensions into a scalar. it initially addresses the case where the faults frequencies are unknown. In addition, the proposed indicator is able to return information for different levels of damages in both stationary and non-stationary operating conditions. A new pre-processing step is provided to ensure an efficient and constant statistical threshold. The proposed indicator is intended to be used in an autonomous process without the need for visual analysis and human interpretation. The proposed indicator is compared with a recent indicator based on the Envelop Spectrum, in terms of classification and detection performance. Several applications using real and benchmarked data eventually illustrate the capability for self-running diagnosis.

Keywords: *spectral coherence, Gaussianity, Stationarity, Acoustic signature, Indicator.*

2 Introduction

Roller bearings (REBs) are one of the essential components of rotating machines, hence the demand for their efficient and reliable condition monitoring (CM). Condition monitoring ensures maximum production, prevents accidents and serious damage and helps to detect failures at an early stage by keeping the system in good conditions. Over the last few decades, considerable research has been conducted on diagnostics based on REB vibrations and acoustics signals leading to the development of some condition's indicators. Therefore, several strategies have been adopted. This is derived from the fact that the occurrence of numerous faults induces changes in signal characteristics that can be described as (i) a deviation from Gaussianity, and/or (ii) a shift in the statistical behavior of the signal from stationary to non-stationary, accompanied by (iii) a change in the machine's acoustic signature.

The crest factor [1], the peak-to-peak, the entropy [2]–[4], the form factor, the third-order central moment (skewness) and the fourth-order central moment (kurtosis) [5], [6], or any higher-order moments or cumulants [7], [8] are all typical examples of the non-Gaussianity measure. They are dedicated to characterizing the non-Gaussian behavior in the form of impulsivity of machine signals. The most traditional and probably the most widely used is the kurtosis, or its combination with other indicators. In the past, they have been used mainly because of their simple calculation formulas, and their relatively

short computation times. This is despite its uncorrelated values with the fault symptoms in numerous situations, reported in many studies[9], [10]. This argument has become obsolete thanks to modern computing capabilities.
The roughness indicator, as traditionally calculated in the time domain from the Aures model [11], is an example of the psychoacoustic parameters used to monitor the existence of a fault based on an alteration of the machine's acoustic signature. It aims to mimic the ability of the human auditory system to detect high-frequency modulation, as evidenced by the faulty rotating machines. The researchers have developed various mathematical models [12]–[15] to estimate roughness but none of them have been normalized.
The degree of cyclostationarity [16] and the indices of cyclostationarity [17] based on the 2nd-order cyclical cumulants or any higher-order cyclostationarity indices based on higher-order cyclical cumulants [18] are typical examples of measures of the non-stationarity that characterizes the cyclostationarity introduced by the fault existence. Despite its importance in diagnosis, the real-time use of CS indices can be hindered in practice by its high cost, especially in real-time applications [19].

This paper aims to fill in these gaps by proposing an indicator sensitive to both non-stationarity, non-Gaussianity and to the modification of the acoustic signature of the vibratory signal. To do so, the frequency domain instead of time domain is used since it better extracts cyclic repetition from a signal produced by a repetitive fault and also reduces the noise impact. The cyclostationary framework is then our subject of interest since it has been reported that rotating machine signals are cyclostationary [20]. Advantage is taken of the availability of a recently proposed fast algorithm to calculate the spectral coherence [19], on which the proposed conditioning indicator is based. The spectral correlation is a three-dimensional distribution of all modulation patterns existing in a signal as a function of the carrier frequency in Hertz and the modulation frequency (also called cyclic frequency) in machine order, which generalizes the SC to nonstationary operations. It is thus considered optimal for revealing bearing fault signatures under stationary and nonstationary speed regimes [21], [22].
The idea is to condensate the whole information initially displayed in the spectral coherence into a scalar after an appropriate weighting performed to select the audible frequencies range from about 20 Hz to 20 kHz and the audible modulations range from about 15 Hz to 200 Hz. This selection can be easily made using the weight $\omega_{k,p}$ designed as a bandpass filter, used to accentuate or reduce certain frequency components in order to model the bandpass characteristic of the roughness on the modulation frequency.
This approaching, the spectral coherence which is sensitive to both non-stationarity and non-Gaussianity, also becomes sensitive to the acoustic signature of the vibratory signal. A new preprocessing step is provided in order to eliminate any possible bias (as typically produced by transient disturbances in the signal or the presence of unexplained nonstationarities) in the estimated spectral coherence. This original step is necessary to produce a pivotal statistic by forcing the spectral coherence to have a constant probability distribution with respect to the dual frequencies plan.
The proposed indicator is statistically consistent, i.e. its variance converges to zero when the signal length increases. On the opposite, Aures' roughness does not involve any time average and is therefore prone to significant estimation errors. Contrary to the kurtosis, the proposed indicator separates impulsivity from non-stationarity, allowing the identification of the type of deviation from normality. A non-nonparametric hypothesis test is also provided in order for this indicator to be credible and possibly implemented in an automated monitoring system. The capacity of the proposed indicator is validated on real data and benchmarked with the kurtosis to extract meaningful conclusions. It is found to return higher performance in terms of detecting faulty bearings.

3 Indicator

3.1 Preliminary steps

This steps briefly resumes the statistical methodology proposed by *kass et al.*[22] to design the test statistics. The starting point is to describe the health of the system under investigation by two alternative hypotheses, H_0 and H_1, which correspond respectively to the healthy and the faulty states, respectively. The principle is to consider the spectral coherence, $\gamma_X^{(1)}(\alpha_l\ ,\ f_k)$, as the random quantity of interest rather than its squared magnitude.

In principle, Under H_0, the random field $\gamma_X^{(1)}(\alpha_l\ ,\ f_k)$, seen as a function of the two frequency variables α_l and f_k, can be shown to have zero probability of being nil at any position $(\alpha_l\ ,\ f_k)$ even though having small values. Under the alternative hypothesis H_1, the difference is that the random field will have higher magnitudes along parallel lines, discretely located at cyclic frequencies associated with the fault frequencies. The objective is to keep only these values and to zero all the other ones. To do so, a statistical threshold, defined as a high percentile, is needed to differentiate between information and background noise. Hence, the presence of a possible bias (as typically produced by transient disturbances in the signal or the presence of unexplained nonstationarities) in the $\gamma_X^{(1)}(\alpha_l\ ,\ f_k)$ compromises the efficiency of the latter threshold. As result, the noise baseline is not uniformly distributed along the frequencies axis. It is therefore impossible to establish a fixed threshold to distinguish between information and noise. To correct this situation, the following empirical steps are proposed. The first step is to standardize the EES in order to force it to have a constant probability distribution with respect to the cyclic order α, under the null hypothesis H_0. In principle, The transformation reads

$$\gamma_X^{(2)}(\alpha_l\ ,\ f_k)\ = \frac{\gamma_X^{(1)}(\alpha_l\ ,\ f_k) - \mathrm{E}\left\{\gamma_X^{(1)}(\alpha_l\ ,\ f_k)|H_0\right\}}{\sqrt{\mathrm{E}\left\{\gamma_X^{(1)}(\alpha_l\ ,\ f_k)^2|H_0\right\} - \mathrm{E}\left\{\gamma_X^{(1)}(\alpha_l\ ,\ f_k)|H_0\right\}^2}} \tag{1}$$

where $\mathrm{E}\{\cdots|H_0\}$ stands for the ensemble averaging operator taken under H_0. One issue is to replace $\mathrm{E}\left\{\gamma_X^{(1)}(\alpha_l\ ,\ f_k)|H_0\right\}$ and $\mathrm{E}\left\{\gamma_X^{(1)}(\alpha_l\ ,\ f_k)^2|H_0\right\}$ in the above equation by estimates obtained from a realization of $\gamma_X^{(1)}(\alpha_l\ ,\ f_k)$ which may either pertain to H_0 or H_1. Since the difference in $\gamma_X^{(1)}(\alpha_l\ ,\ f_k)$ under the null and alternative hypotheses is essentially marked by the presence of parallel lines, it is proposed to estimate $\mathrm{E}\left\{\gamma_X^{(1)}(\alpha_l\ ,\ f_k)|H_0\right\}$ from a running median of $\gamma_X^{(1)}(\alpha_l\ ,\ f_k)$, called $\mu_{MED}(\alpha_k)$, and $\mathrm{E}\left\{\gamma_X^{(1)}(\alpha_l\ ,\ f_k)^2|H_0\right\}$ from the running median of the absolute deviation, called $\sigma_{MAD}(\alpha_k)$. The rationale for using a running median is to leave unaffected informative peaks in the spectral coherence. Therefore, the $\gamma_X^{(2)}(\alpha_l\ ,\ f_k)$ reads

$$\gamma_X^{(2)}(\alpha_l\ ,\ f_k)\ =\ \frac{\gamma_X^{(1)}(\alpha_l\ ,\ f_k) - \mu_{MED}(\alpha_l, f_k)}{\sigma_{MAD}(\alpha_l, f_k)} \tag{2}$$

which returns a “pivotal” statistics (i.e. whose probability distribution does not depend on any unknown parameter). Briefly, the presence of the possible bias is firstly removed by subtracting a running median, then the results are standardized by dividing it with a running median of the absolute deviation. These two steps can be though as a normalization of the H_1 statistics with respect to the H_0 statistics.

3.2 Proposition

The first step is to preserve the informative values, i. e. the spectral lines parallel to the frequency axis f_k along α_l, expected during the fault’s existence i. e. under H_1.To do so, this step consists of setting all non-significant peaks in $\gamma_X^{(2)}(\alpha_l\ ,\ f_k)$ to zero which are found below a given threshold. A reasonable choice is

to define the threshold as a high percentile p_c (e.g. $p_c = 0.9$)[23], which means that only the $100(1 - p_c)\%$ highest values will be kept. Thanks to the standardization step, the threshold is constant over the full frequency plane $(\alpha_l\ ,\ f_k)$. And the $\gamma_X^{(3)}(\alpha_l\ ,\ f_k)$ is expressed as

$$\gamma_X^{(3)}(\alpha_l\ ,\ f_k) = \gamma_X^{(2)}(\alpha_l\ ,\ f_k).\mathbb{I}_{\left[\gamma_X^{(2)}(\alpha_l\ ,\ f_k)>p_c\right]} \tag{3}$$

where the symbol $\mathbb{I}_{\left[\gamma_X^{(2)}(\alpha_l\ ,\ f_k)>p_c\right]}$ denotes the indicator function defined on the frequencies plane $(\alpha_l\ ,\ f_k)$ having the value 1 for all elements of $(\alpha_l\ ,\ f_k)$ satisfying the condition $\gamma_X^{(2)}(\alpha_l\ ,\ f_k) > p_c$ and the value zero otherwise.

This is a crucial step as the next step involves modelling the bandpass characteristics of the roughness by accentuating or reducing certain frequency components, thus preventing the occurrence of misleading peaks.

The next step is to performs an appropriate weighting of the $\gamma_X^{(3)}(\alpha_l\ ,\ f_k)$ so as to select the audible frequencies range from about 20 Hz to 20 kHz and the audible modulations range from about 15 Hz to 200 Hz in order to approach the roughness measurement proposed by Aures. This selection can be easily realized based on the weight $\omega_{k,p}$ designed as a bandpass filter, used to accentuate or reduce specific frequency components in order to model the roughness bandpass characteristic on modulation frequencies. In other words, $\omega_{k,p}$ resembles the distribution matrix of the weighting functions for each *Bark* channel. The weighting of $\gamma_X^{(3)}(\alpha_l\ ,\ f_k)$ is achieved as follows:

$$\gamma_X^{(4)}(\alpha_l\ ,\ f_k) = \gamma_X^{(3)}(\alpha_l\ ,\ f_k).\omega_{k,p} \tag{4}$$

The third step is divided into two sub-steps, the first is to integrating the $\gamma_X^{(4)}(\alpha_l\ ,\ f_k)$ over the cyclical frequency axis α_l, which condenses the whole information initially displayed in three dimensions into a two-dimensional representation,

$$I_X^{(5)}(\ f_k) = \frac{1}{F_1}\left[\sum_{l\in F_1} \gamma_X^{(4)}(\alpha_l\ ,\ f_k)\right] \tag{5}$$

While the second sub-step consists of dividing the frequency axis into a *Bark* filter bank to estimate the modulation depth per auditory channel which is spaced by 1 *Bark* representing a psychoacoustic scale for the bandwidths of the hearing filters. The latter is a frequency band established by Zwiker [24], it is divided into 24 critical bands ranging from 0 to 15500 Hz.

As a final step, the roughness dependence with respect to the carrier frequency is introduced into the model by multiplying $I_X^{(5)}(\ f_k)$ by a weighting function $g(f_k)$ with factors ranging from 0.6 to 1.1 in accordance with the dependency of the roughness to the carrier frequency of the amplitude modulated tones. The values of the weighting function with respect to the channel number are shown in Figure 1.

Finally, the proposed indicator I_R is obtained by integrating $I_X^{(5)}(\ f_k)$ over the frequency axis f_k.

$$I_R = \frac{1}{F_2}\sum_{k\in F_2} I_X^{(5)}(\ f_k)\ .\ g(f_k) \tag{6}$$

By analogy with the result given by the connection between the kurtosis and the sum of the squared envelope spectrum [25], it was shown in [23] that the proposed indicator might be interpreted as a kurtosis, yet sensitive only to cyclostationary components.

The next section describes how the fault detection will be done using a statistical hypothesis test using the proposed indicator. In this context, alternative strategies to statistical testing can also be used. For example, the proposed indicator can also be used as an input parameter for an SVM classifier (machine

vector support) or a neural network. This statement is based on the observation of the results obtained by applying the proposed indicator to the various databases.

3.3 Hypothesis testing, design

The interpretation of the proposed indicator could vary from one application to another, depending on several parameters (such as the noise level related to transient perturbations in the signal or to the presence of unexplained non-stationarity as well as the vibration level and the interfering contribution of other second-order components emitted by other sources). In the majority of the literature [16]–[18], the provided methods give their results as scalar. The latter indicates the presence of a fault in some applications while in another, and for the same value, the fault will be considered as absent. This is why a threshold is needed for decision-making. To do so, two thresholds are provided in this paper. The lower threshold I_L is defined as the indicator value of the randomized version of the vibration signal under which the fault is absolutely absent. In detail, I_L is equal to the indicator value when the signal is randomized. The randomization of the signal is defined as a circular permutation of its elements, it can be performed using the MATLAB function called "randperm". The latter returns a new version of the signal containing a random permutation of its values. On the other hand, the link between the kurtosis and the spectral correlation makes it possible to reach the upper threshold, I_U, beyond which the fault presence is declared with high certainty.

After the I_U is calculated, a comparison is then made with the proposed indicator to detect the fault presence. If I_R has a value greater than I_U, the fault exists.

The null hypothesis test relative to our case originating from the comparison between I_R and I_U can be written as:

“Reject the null hypothesis H0 if:

$$I_R \geq I_U \tag{7}$$

where $I_U \geq 2 \times I_L$.

It easily allows performing a statistical test: according to the decision rule, any value of I_R that is greater than the I_U-threshold will indicate that the signature of the fault is detected. The proof of proposition Eq. (7) is based on observing that under the null hypothesis test H_0 the quantity asymptotically follows a nonparametric distribution that has a constant bias and variance all over the cyclic order axis. It also remembers that this test is true almost everywhere.

The complete flow diagram for the algorithm described in this section is shown in Fig.3

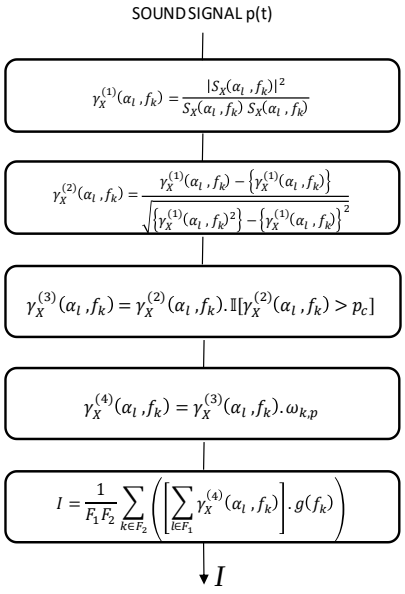

Figure 1.Complete algorithm flowchart

It is worth noting that I_R is very similar to the Aures' roughness measure used in psychoacoustics. One difference is that Aures' roughness is based on a decomposition of the signal through a Bark filter bank whereas a narrow-band decomposition is used in this paper, yet this is more or less transparent after integration over the frequency plane $(\alpha_l\ ,\ f_k)$. Another difference is that Aures' roughness does not involve any time average and is therefore prone to significant estimation errors. On the contrary, the indicators introduced in this work are statistically" consistent" (i.e. their variances converge to zero when the signal length increases).

4 Experimental Validation

The ability of any method in detecting a bearing fault must be validated on real signals. In the present paper, four benchmarks are used. The first is provided by the Case Western Reserve University (CRWU) bearing data center [26], while the second is an industrial database provided by SOMFY-Cluse. These databases are widely used to test new algorithms by comparing their efficiency with existing techniques [27]. The CRWU's database provides multiple fault types, i.e. rolling element, cage inner-race, and outer-race fault, and it is used to illustrate the proposed method and to compare the proposed algorithm to those existing in the literature. The industrial database is used to illustrate the diagnosis of bearings in a real industrial world signal.

4.1 Algorithm illustration and comparison with kurtosis

To illustrate the proposed algorithm, we consider a real industrial signal. This analyzed signal is provided by Somfy and includes an industrial fault. It is provided as supplementary material of the article. This may be used as a general source of bench mark data for research on diagnosis of industrial faults under constant speed operation. The comparing the results of the proposed indicator with those given by kurtosis. The duration of signals is 20 s with a sampling frequency of 50 kHz.

As explained above, the first begins with the calculation of the fast estimator of the spectral coherence for the resampled time domain signal $\gamma_X^{(1)}(\alpha_l\ ,\ f_k)$. In what follows, the window length in the Fast-OFSC is set to $Nw = 2^9$ in order to achieve a frequency resolution of about 100 Hz and the cyclic range $\alpha_{max} = 750$ Hz. The next step is to standardize $\gamma_X^{(1)}(\alpha_l\ ,\ f_k)$ in order to force it to have a constant probability

distribution with respect to the frequency plane, under H_0. The statistical threshold will be defined as a high P_c percentile ($P_c = 0.9$), which means that only the $100(1 - P_c)\%$ of the highest values will be preserved. It is noteworthy that this method perfectly preserves the diagnostic information that nicely appears with a significant overrun of the 0,1% statistical threshold. This signal is easily diagnosable and it should, therefore, be considered as a preliminary test for the proposed algorithm. The visual inspection of the spectral coherences presented in Figure 2 (a) and (b) shows a series of symptomatic pulses at the fault frequency - spectral lines parallel to the *f-axis* discretely located at cyclic frequencies associated with the fault frequencies- as expected by the model given by Somfy during under H_1. In Figure 2 (b) it is obvious that some frequency components disappear from the $\gamma_X^{(1)}(\alpha_l\,,\,f_k)$ while retaining only informative peaks and eliminating noise-related components found below the chosen threshold.

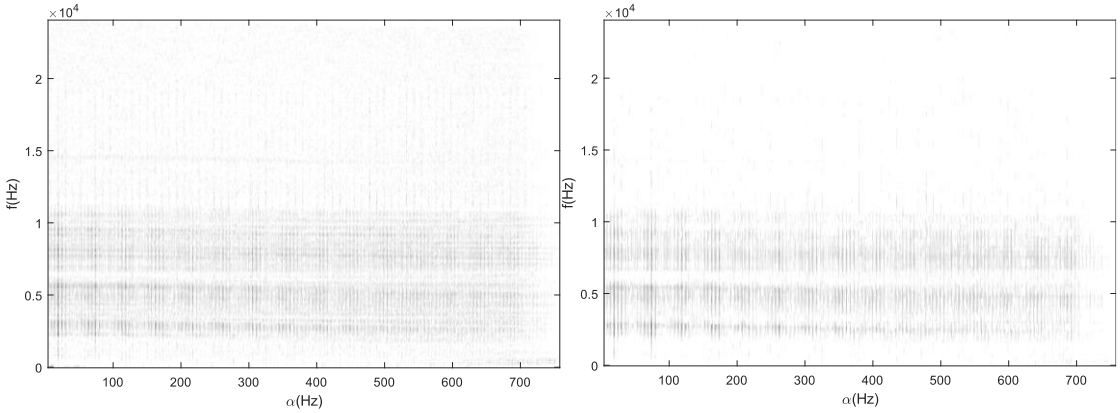

Figure 2. For the raw time signal a) the $\gamma_X^{(1)}(\alpha_l\,,\,f_k)$, and b) the $\gamma_X^{(3)}(\alpha_l\,,\,f_k)$

The audible frequencies and modulations range are selected by using the weight $\omega_{k,p}$, shown in Figure 3(a), so as to select the audible frequencies range from about 20 Hz to 20 KHz and the audible modulations range from about 15 Hz to 200 Hz. The weighted version of spectral coherence $\gamma_X^{(4)}(\alpha_l\,,\,f_k)$ is presented in Figure 3 (b). As shown in Figure 3 (b), certain frequency components are emphasized or reduced so as to model the band-pass characteristic of the roughness over the modulation frequency.

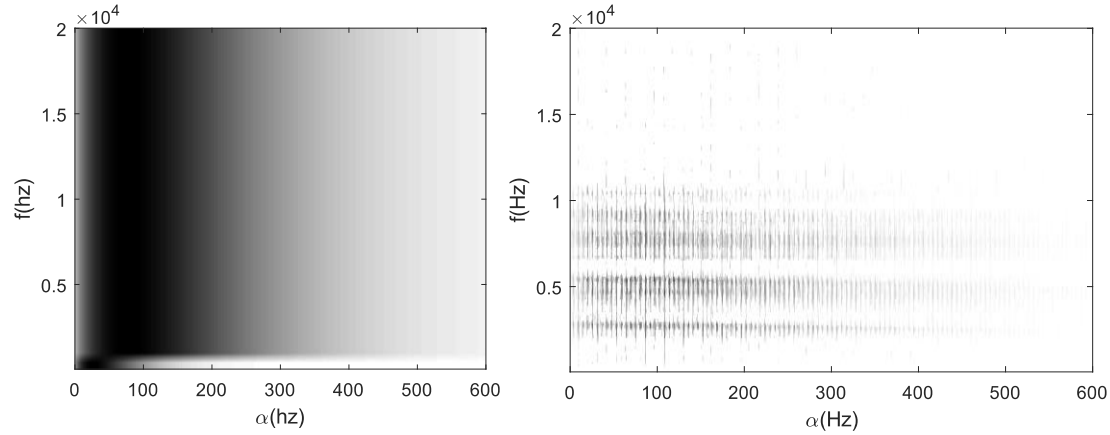

Figure 3 (a) The weight $\omega_{k,p}$ used to select the audible frequencies and modulations ranges, (b) the $\gamma_X^{(4)}(\alpha_l\,,\,f_k)$.

In the next step and as mentioned in section 3.2, the integration of $\gamma_X^{(4)}(\alpha_l\,,\,f_k)$ over α_k will be performed. The two-dimensional representation $I_X^{(5)}(\,f_k)$ which condenses the three-dimensional information is shown in Figure 4 (a). Then, the modulation-depth per auditory channel is estimated by

dividing the f-axis into the 24 bands of Bark filter. $I_X^{(5)}(f_k)$ is then multiplied by a weighting function $g(f_k)$. Finally, the roughness indicator I_R is obtained by integrating the weighted $I_X^{(5)}(f_k)$ over the f-axis. The latter has in this case a value of 2.2624.

The signal is now randomized in order to calculate the upper and the lower threshold. Figure 4 (a) et (b) shows both the raw time signal and its normalized version. When both signals are visually inspected, it is evident that cyclostationary symptoms are lost when the signal is randomized, which is consistent with the auditory test performed using MATLAB's sound function (). More precisely, when performing a hearing test, the original signal exhibits periodic behavior that is produced with each cycle. This periodic symptom is no longer heard after the randomization of the signal. The value of the indicator in this case $I_L = 0.27109$ is negligible compared to the case of existing fault, matching both the visual and the hearing inspection. I_R is equal to about 10 times I_L. According to the decision rule provided by Eq. (7), the fault existence is reported.

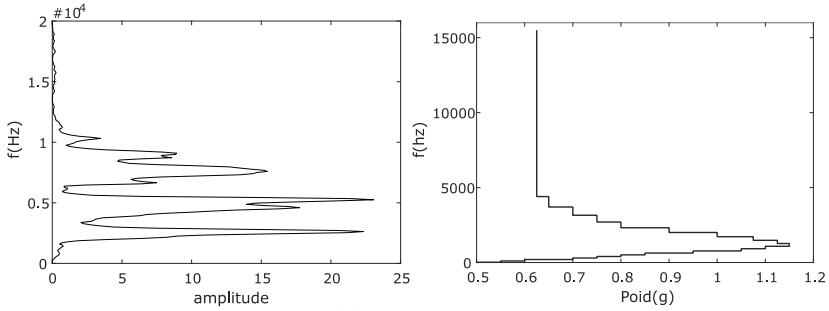

Figure 4. (a) the integration of $\gamma_X^{(4)}(\alpha_l, f_k)$ over α_l, (b) the weighting function g

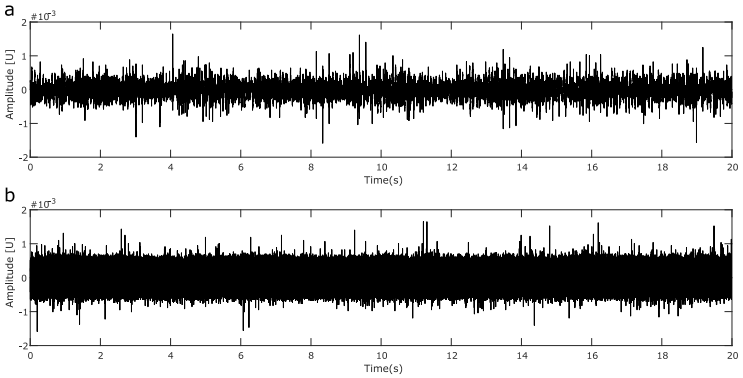

Figure 5. (a) the raw time signal and (b) its randomized version

Surprisingly, and contrary to both visual and auditory inspection tests, the kurtosis of the original and randomized signal gives a very low value of 3.0088 reporting the fault absence in both cases.

After an appropriate filtration of the raw time signal, the kurtosis value is now 20.8589, corresponding to a very high value -7 times the value of a normal case - indicating the failure's presence. The success of kurtosis after proper filtering highlights its limitation when analyzing a signal with a low signal-to-noise ratio and at the same time demonstrating the superiority of the indicator designed from a cyclostationary method for the detection of fault symptoms.

Now the filtered signal is randomized to study kurtosis response in this case and presents another superiority of the proposed indicator over kurtosis. In detail, the same kurtosis value for both the randomized signal and the filtered signal is obtained indicating that the fault is detected in these cases. The obtained results are expected since kurtosis is defined as follows

$$k = \frac{\frac{1}{n}\sum_{i=1}^{n}(x_i - \bar{x})^4}{\left(\frac{1}{n}\sum_{i=1}^{n}(x_i - \bar{x})^2\right)^2} \quad (8)$$

This equation shows that regardless the sequence of this signal summation, results will be the same since the permutation disorganizes only the sequence of the original signal. The kurtosis in this case cannot therefore indicate whether the signal is cyclostationary or stationary but not Gaussian. On the other hand, the proposed indicator can perform this distinction giving a cyclic roughness value of 2.2424 for the filtered signal and 0.25819 for its randomized version.

4.2 Performance Evaluation in the CWRU database

The performance of the proposed indicators is now evaluated on the bearing signals provided by the CWRU database. The CWRU database has been used in many references (e.g. [19], [22], [27], [28]) and can be considered as a reference to test newly proposed algorithms and compare them against the state-of-the-art. The experimental setup consists of a 1.4914 kW, reliance electric motor driving a shaft on which a torque transducer and encoder are mounted. Torque is applied to the shaft via a dynamometer and electronic control system. Four types of vibration signals are collected (normal, ball fault, inner-race fault, and outer-race fault), acquired by accelerometer sensors under different operating loads and speeds. More details about the test bench as well as the description of its vibration signals can be found in the reference source [27]. In this study, the drive end data-set category with sampling frequency 48 kHz have been analyzed. Information for all 64 data sets used are shown in table 1. The capacity of the proposed indicator is evaluated using different faults types. The $\gamma_X^{(1)}(\alpha_l\ ,\ f_k)$ parameters are as given in the previous section.

Table 1. The 48K drive end bearing faults data sets used.

Fault types	Data sets name
Inner-race	110,111,112,174,176,177,14,215,217
Outer-race (centered)	135,136,137,138,201,203,204,238,239,240,241
Normal data	97,98,99,100

Table 2 and table 4 collect the results of the proposed method. Included in these tables are the I_R as well as the *kurtosis* values, of each raw time signal and its randomized version.

As shown in Table 3, for the original signals, I_R is close to 0.15, while for its randomized version, it is about 0.1 ($I_L = 0.1$). In all these cases and in according to the decision rule in equation (7), the fault is declared missed. The kurtosis in these cases is approximately 3. From Table 3, nearly the same increasing or decreasing behavior of the proposed indicator values are detected compared to the values provided by kurtosis and by the roughness indicator provided in commercial psychoacoustic software. In all these cases and in according to the decision rule in equation (7), the fault is declared presented. According to the obtained results, all faults detected by the human visual inspection of [27] in the inner ring and outer ring are also detected by the proposed indicator. It is clearly proven that the distinction between healthy and defective bearings can be made using these indicators. Unfortunately, given that the proposed indicator provides overlapping values when applied to the different types of bearing faults, the existence of the fault can be detected but not identified.

In conclusion, the objective has been achieved and the proposed indicator can identify the fault even if its frequencies are unknown.

Table 2. analysis results of the healthy bearing; Kurtosis, I_R

	Raw signal	Randomized signal

Dataset	*kurtosis*	I_R	*kurtosis*	I_L
100	2.9572	0.1354	2.9572	0.0999
97	2.7642	0.1471	2.7642	0.1011
98	2.9306	0.1422	2.9306	0.1002
99	2.9306	0.1422	2.9306	0.0977

Table 3. analysis results of the faulty bearing; Kurtosis, I_R

Inner-race faults				
	Raw signal		Randomized signal	
Dataset	*kurtosis*	I_R	*kurtosis*	I_L
110	7.36862	0.494821	7.36862	0.101008
111	7.51043	0.467891	7.51043	0.103501
112	6.82779	0.439782	6.82779	0.104584
174	11.6689	0.504829	11.6689	0.10279
176	20.1511	0.861307	20.151	0.117898
177	14.9400	0.823425	14.940	0.114356
214	3.93724	0.507309	3.93724	0.100236
215	3.65185	0.444887	3.65185	0.099826
217	3.65185	0.444887	3.65185	0.09756
Outer-race faults (Centered)				
	Raw signal		Randomized signal	
Dataset	*kurtosis*	I_R	*kurtosis*	I_L
135	6.7415	0.5032	6.741461	0.1047
136	6.8648	0.5293	6.864769	0.1027
137	6.9370	0.5295	6.937026	0.1017
138	7.3917	0.5154	7.391694	0.1030
201	3.7676	0.2039	3.767617	0.1031
203	6.0172	0.2108	6.017181	0.1015
204	2.9993	0.2104	2.999284	0.0996
238	20.7910	2.3374	20.79105	0.1169
239	20.5436	2.7322	20.54365	0.1148
240	21.0265	0.5032	21.02651	0.1205
241	19.7818	0.5293	19.78182	0.1199

5 Conclusion

This paper aims introduces an autonomous method of bearing diagnosis. It relies on the introduction of a new scalar indicator. The indicator results from a post-processing of the spectral coherence, as computed by the fast algorithm.

The factors that are likely to impede the autonomous diagnosis have been addressed; a new standardization of the estimated spectral coherence to remove any possible bias and frequency dependence in the estimation variance. The method comes with a robust hypothesis test, which is crucial for decision making.

The proposed method has been validated on several databases, where it has been checked to be able to systematically replace both the human intervention or the classical conditioning indicator to efficiently complete the diagnosis of bearings.

6 References

[1] J. Igba, K. Alemzadeh, C. Durugbo, and E. T. Eiriksson, “Analysing RMS and peak values of vibration signals for condition monitoring of wind turbine gearboxes,” *Renew. Energy*, vol. 91, pp. 90–106,

2016.

[2] R. Yan and R. X. Gao, “Approximate entropy as a diagnostic tool for machine health monitoring,” *Mech. Syst. Signal Process.*, vol. 21, no. 2, pp. 824–839, 2007.

[3] H. Hong and M. Liang, “Fault severity assessment for rolling element bearings using the Lempel–Ziv complexity and continuous wavelet transform,” *J. Sound Vib.*, vol. 320, no. 1–2, pp. 452–468, 2009.

[4] J. Antoni, “The infogram: Entropic evidence of the signature of repetitive transients,” *Mech. Syst. Signal Process.*, vol. 74, pp. 73–94, 2016.

[5] A. Rai and S. H. Upadhyay, “A review on signal processing techniques utilized in the fault diagnosis of rolling element bearings,” *Tribol. Int.*, vol. 96, pp. 289–306, 2016.

[6] C. Pachaud, R. Salvetat, and C. Fray, “Crest factor and kurtosis contributions to identify defects inducing periodical impulsive forces,” *Mech. Syst. Signal Process.*, vol. 11, no. 6, pp. 903–916, 1997.

[7] M. Cocconcelli, G. Curcurú, and R. Rubini, “Statistical evidence of central moment as fault indicators in ball bearing diagnostics,” in *The International Conference Surveillance 9*, 2017.

[8] H. R. Martin, “Statistical moment analysis as a means of surface damage detection,” in *Proceedings of the 7th international modal analysis conference*, 1989, vol. 1, pp. 1016–1021.

[9] J. Antoni and P. Borghesani, “A statistical methodology for the design of condition indicators,” *Mech. Syst. Signal Process.*, vol. 114, pp. 290–327, 2019.

[10] R. B. Randall, J. Antoni, and K. Gryllias, “Alternatives to kurtosis as an indicator of rolling element bearing faults,” in *Proceedings of ISMA2016 International Conference on Noise and Vibration Engineering*, 2016, pp. 2503–2516.

[11] W. Aures, “Ein berechnungsverfahren der rauhigkeit,” *Acta Acust. united with Acust.*, vol. 58, no. 5, pp. 268–281, 1985.

[12] P. Daniel and R. Weber, “Psychoacoustical roughness: Implementation of an optimized model,” *Acta Acust. united with Acust.*, vol. 83, no. 1, pp. 113–123, 1997.

[13] P. N. Vassilakis, “Auditory roughness as a means of musical expression,” *Sel. Reports Ethnomusicol.*, vol. 12, no. 119–144, p. 122, 2005.

[14] M. Leman, “Visualization and calculation of the roughness of acoustical musical signals using the synchronization index model (SIM),” in *Proceedings of the COST G-6 Conference on Digital Audio Effects (DAFX-00), December*, 2000, pp. 7–9.

[15] R. Duisters, “The modeling of auditory roughness for signals with temporally asymmetric envelopes.” Master’s thesis, Technische Universiteit Eindhoven, Eindhoven, The Netherlands, 2005.

[16] G. D. Živanović and W. A. Gardner, “Degrees of cyclostationarity and their application to signal

detection and estimation," *Signal Processing*, vol. 22, no. 3, pp. 287–297, 1991.

[17] P. PRIEUR and G. D'URSO, "Des indices de cyclostationnarité pour la surveillance des engrenages," in *15° Colloque sur le traitement du signal et des images, FRA, 1995*, 1995.

[18] A. Raad, J. Antoni, and M. Sidahmed, "Indicators of cyclostationarity: Theory and application to gear fault monitoring," *Mech. Syst. Signal Process.*, vol. 22, no. 3, pp. 574–587, 2008.

[19] J. Antoni, G. Xin, and N. Hamzaoui, "Fast computation of the spectral correlation," *Mech. Syst. Signal Process.*, vol. 92, pp. 248–277, 2017.

[20] J. Antoni, "Cyclic spectral analysis in practice," *Mech. Syst. Signal Process.*, vol. 21, no. 2, pp. 597–630, 2007.

[21] D. Abboud, "Vibration-based condition monitoring of rotating machines in nonstationary regime," 2015.

[22] S. Kass, A. Raad, and J. Antoni, "Self-running bearing diagnosis based on scalar indicator using fast order frequency spectral coherence," *Measurement*, vol. 138, pp. 467–484, 2019.

[23] J. Antoni, P. Borghesani, S. Kass, A. Raad, and K. Gryllias, "Methodologies for designing new condition indicators," in *Proceedings of ISMA 2018-International Conference on Noise and Vibration Engineering and USD 2018-International Conference on Uncertainty in Structural Dynamics*, 2013, pp. 883–890.

[24] E. Zwicker and H. Fastl, "Psychoacoustics: Facts and Models. 1990." Springer-Verlag.

[25] P. Borghesani, P. Pennacchi, and S. Chatterton, "The relationship between kurtosis-and envelope-based indexes for the diagnostic of rolling element bearings," *Mech. Syst. Signal Process.*, vol. 43, no. 1–2, pp. 25–43, 2014.

[26] "The Case Western Reserve University Bearing Data Center Website." [Online]. Available: https://csegroups.case.edu/bearingdatacenter/.

[27] W. A. Smith and R. B. Randall, "Rolling element bearing diagnostics using the Case Western Reserve University data: A benchmark study," *Mech. Syst. Signal Process.*, vol. 64, pp. 100–131, 2015.

[28] W. Li, M. Qiu, Z. Zhu, F. Jiang, and G. Zhou, "Fault diagnosis of rolling element bearings with a spectrum searching method," *Meas. Sci. Technol.*, vol. 28, no. 9, p. 95008, 2017.